Chapter 7

Seismic Behaviour of Monolithic Objects: A 3D Approach

Alessandro Contento, Daniele Zulli and
Angelo Di Egidio

Additional information is available at the end of the chapter

http://dx.doi.org/10.5772/54863

1. Introduction

Despite the many progresses done in the modelling of rigid blocks, the grounding work for most of the research in this field remains [1], where a 2D model of the rigid block is obtained and the rocking and slide-rocking approximated conditions are written. Following papers on the dynamics of rigid bodies can be divided in two main groups, according to the kind of excitation used: earthquake excitation or sine-type pulse excitation (mainly one-sine). To the first group belong [2-5], in the second one, [6-10] can be found. In time, models of rigid blocks, very useful in many research fields, have been increased in complexity. Recently, for instance, sliding phenomena and the eccentricity of the center of mass have been considered (see [3, 11]). Some papers have been focused to specific problems, for example in [12] the behavior of two stacked rigid blocks has been considered, whereas in [13, 14] the attention has been pointed to blocks on flexible foundations. The dynamics and control of 2D blocks have also been analyzed in the framework of the bifurcation theory in [15, 16, 17].

The effects of the simultaneously presence of horizontal and vertical base excitations have been considered in some papers. For example, in [12, 18, 19] different problems related to the overturning of bi-dimensional rigid blocks have been studied in details.

Lately a large interest has been given to models of rigid bodies with base isolation systems, in order to improve the safety of art objects (see [20-22]). It has been proved that, in certain ranges of geometrical parameters of the rigid block, the effectiveness of base isolation can be amplified when coupling the isolating systems with devices able to limit the displacement of the oscillating base, so as to prevent the falling of the base of the body (see [23, 24]).

Recently, 3D models, mostly circular based, have been used in particular research fields, more precisely to study motions of a disk of finite thickness ([25, 26]), the wobbling of a frustum ([27]) or the sloshing in a tank ([28]).

A three-dimensional model of rigid body with a rectangular base, able to rock around a side or a vertex of the base, already presented by the authors in [29], is used herein to further study the dynamic behavior of rigid blocks. In particular the effects of a vertical one-sine excitation, acting concurrently to the horizontal one, and the seismic response of rigid bodies are considered. The body can experience only rocking motion since it is herein assumed that it possesses a slenderness for which bouncing is not triggered (see [22, 23]). Eccentricity of the center of mass, evaluated with respect to the geometrical center of the parallelepiped that ideally circumscribes the body, is also considered. The equations of motion of the body are obtained making use of the balance of moments. Impacts between the base and the ground are treated by imposing the conservation ofthe angular momentum before and after the impact. Starting conditions of rocking motion around a side or a vertex of the base are obtained by balancing the overturning moments and the resisting moments. Results are obtained by numerical integration of the equations of motion by using a IMSL routine developed in Fortran [30].

Rocking and overturning curves that furnish the amplitude of the one-sine pulses able to uplift or to overturn the body, versus the angular direction of the horizontal excitation, are obtained. The role of the period of the excitations, the geometrical characteristics of the body and the eccentricity of the center of mass are also highlighted. Particular attention is focused to the relative phase between the horizontal and vertical excitations. The presence of the vertical pulse can strongly change the behavior of the system with respect to the case where only the horizontal excitation is considered.

Regarding the seismic excitation, three different registered Italian earthquakes, with different spectrum characteristics, are used in the analyses. Two type of analyses are performed in the paper: the first is conducted by varying the direction of the seismic input to point out if, for some directions, the 3D model of rigid block furnishes more accurate results than the classical 2D models; the second is performed by fixing the direction of the input with the aim to highlight the role of the mechanical and the geometrical characteristics of the rigid block in the seismic response. Also in this case, rocking and overturning curves, that furnish the amplitude of the seismic excitation able to uplift or to overturn the body versus the angular direction of the excitation, are obtained. The role of the type of spectrum of the seismic excitation, the geometrical and mechanical characteristics of the body and the eccentricity of the mass center are also highlighted.

Finally, almost all the figures in the paper refer to a well-known statue. It is taken as example of the use of the model here discussed, but there are many other possible applications.

2. Description of the considered mechanical system

The base of the rigid block is supposed to be rectangular, with the four vertices indicated as A, B, C, D (see Fig. 1). The block is circumscribed by an ideal parallelepiped with upper vertices E, F, H, I, and lower vertices coinciding with A, B, C, D. The point M is the the centroid of the parallelepiped, while G is the centroid of the block.

When the body is at rest, at the $t = t_0$ initial time, the position vector of a generic point with respect the i-th vertex ($i = A,\ B,\ C,\ D$) is indicated as $\hat{\mathbf{r}}_i$ and the position vector of the other three

http://dx.doi.org/10.5772/54863

vertices with respect to the vertex i is indicated as $\hat{\mathbf{r}}_{ij}(t)$ ($i=A, B, C, D, j\neq i$). The body is allowed to rotate alternatively around one of the vertices, being this vertex in contact with the coordinate plane $z=0$. If the body is rocking about the i-th vertex (see Fig. 1_e for $i=C$), the position vector rotates about the vertex; its time evolution is described by

$$\mathbf{r}_i(t) = \mathbf{R}(t)\hat{\mathbf{r}}_i \tag{1}$$

where $\mathbf{R}(t)$ is the 3D finite rotation matrix which can be written in terms of three time-depending angles $\vartheta_1(t)$, $\vartheta_2(t)$, $\vartheta_3(t)$ (see Appendix for a representation of the matrix $\mathbf{R}$). Therefore the total acceleration of the generic point with respect to a fixed frame is written as

$$\mathbf{a} = \mathbf{a}_g - \mathbf{g} + \ddot{\mathbf{R}}\hat{\mathbf{r}}_i \tag{2}$$

where $\mathbf{a}_g$ is the ground acceleration, $\mathbf{g}$ is the gravity acceleration and the dot stands for time differentiation. If the mass per volume of the block is indicated as ρ, the total volume force acting on the generic point of the block during the rocking motion around the vertex i is $f=\rho\mathbf{a}$, which becomes, using Eq. (2),

$$\mathbf{f} = \rho(\mathbf{a}_g - \mathbf{g} + \ddot{\mathbf{R}}\hat{\mathbf{r}}_i) \tag{3}$$

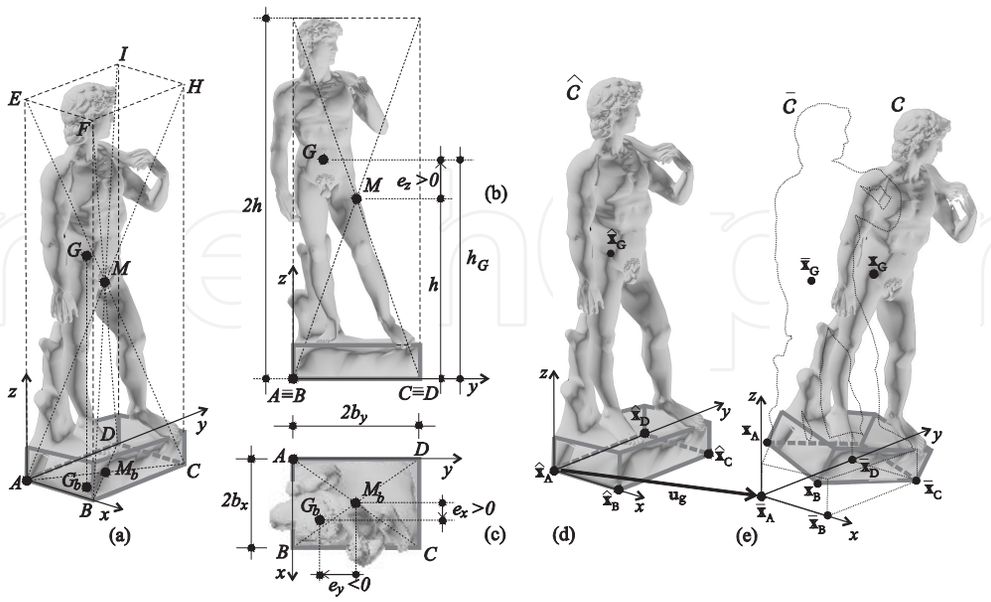

Figure 1. Geometrical characteristics of the rigid block: (a) three-dimensional view; (b) x-z plane projection; (c) x-y plane projection; (d-e) displacements of the rigid block: 3D rocking.

3. General formulation

3.1. Equations of motion

The equations of motions have been already presented in [29], where they are obtained imposing the balance of the moments acting on the body. In particular, when the body is rocking around the i-th vertex, which is assumed to lie on the horizontal, coordinate plane $z=0$, and is identified by its initial position $\hat{\mathbf{x}}_i(t)$, $i=A,\ B,\ C,\ D$, the equations of motion read

$$\mathrm{skw}\left(\hat{\mathbf{s}}_i \otimes (\mathbf{a}_g(t) - \ddot{\mathbf{R}}(t)(\hat{\mathbf{x}}_i - \hat{\mathbf{x}}_A) - \mathbf{g})\mathbf{R}^T(t) - \ddot{\mathbf{R}}(t)\hat{\mathbf{J}}_{iA}\mathbf{R}^T(t)\right) = \mathbf{O} \tag{4}$$

where $\hat{\boldsymbol{s}}_i := \int_{\hat{C}} \rho(\hat{\mathbf{x}} - \hat{\mathbf{x}}_i)dV$ is the vector of (initial) static moment of the body with respect to the vertex i ($\hat{\mathbf{x}}$ is the initial position of a generic point of the block); $\otimes$ is the tensor product; $\mathbf{a}_g(t)$ is the imposed base acceleration vector; $\mathbf{R}(t)$ is the 3D rotation matrix, which in turn depends on three angles $\vartheta_1(t),\ \vartheta_2(t),\ \vartheta_3(t)$; $\hat{\boldsymbol{J}}_{iA} := \int_{\hat{C}} \rho(\hat{\mathbf{x}} - bh_i) \otimes (\hat{\mathbf{x}} - \hat{\mathbf{x}}_A)dV$ is the (initial) Euler tensor with respect to the vertices i and A; $\mathbf{g}$ is the gravity acceleration vector; the superscript T stands for transpose and the dot for time derivative; skw() is the skew part of the tensor in argument (see Fig. 1 and, for details, [29]). In Appendix A all the tensor and the vector quantities appearing in Eq. (4) are explicitly written, to make possible the reproduction of the numerical simulations reported in the following sections. Equations (4) reduce to the special case of 2D motion of the block around a side of the base (the same equation in [22]), when $\mathbf{R}(t)$ describes a planar rotation around one of the coordinate axes x or y.

3.2. Starting and ending conditions

The rigid block is assumed to be in a full-contact condition with the ideal horizontal support at the beginning of the base excitation. The rocking phase begins when the rigid block uplifts. An uplift occurs when the resisting moment M_r due to the weight of the body and to the vertical external acceleration is smaller than the overturning moment M_o due to the horizontal inertial forces. The uplift can occur around a side of the rectangular base (2D rocking motion) or around one of the four lower vertices of the base (3D rocking motion).

The eccentricity of the mass center with respect to the geometrical center of the parallelepiped, when considered, is obtained by introducing a concentrated mass $m_E = \beta m$ and, however, always keeping the total mass m of the body constant. Referring to Fig. 1, the following nondimensional eccentricities are introduced to characterize the system:

$$\varepsilon_x = \frac{e_x}{b_x};\ \varepsilon_y = \frac{e_y}{b_y};\ \varepsilon_z = \frac{e_z}{h} \tag{5}$$

and the slendernesses:

http://dx.doi.org/10.5772/54863

$$\lambda_x := \frac{h_G}{b_y} = \frac{h}{b_y}(1+\varepsilon_z); \lambda_y := \frac{h_G}{b_x} = \frac{h}{b_x}(1+\varepsilon_z) \tag{6}$$

where $2b_x$, $2b_y$, $2h$ are the lengths of the three edges of the parallelepiped, respectively, e_x, e_y, e_z are the components of the distance vector between the center of mass of the body and the center of the parallelepiped, and $h_G = h + e_z$.

3.2.1. Starting condition of 2D rocking

An initial uplift around a side of the rectangular base leads to a 2D motion. In this case a rocking motion takes place when the overturning moment is equal or greater than the resisting moment, due to the vertical component of the acceleration $\ddot{u}_z$ of the center of mass. An initial uplift around a side parallel to the x direction (AB in Fig. 2_a) is considered. Similar conditions can be found for the orthogonal directions, since the mechanical system is symmetric. Thus the uplift occurs when:

$$M_o = ma_{g_y} h_G = M_r = m\ddot{u}_z(b_y + e_y) \tag{7}$$

where a_{g_y} is the component of the ground acceleration along y. Using nondimensional quantities, Eq. (7) reads:

$$\frac{\ddot{u}_y}{\ddot{u}_z} = \frac{1+\varepsilon_y}{\lambda_x}. \tag{8}$$

3.2.2. Starting condition of 3D rocking

An uplift on a vertex can occur either during a 2D rocking motion or directly from the full contact phase. In both cases a 3D motion is obtained.

In order to uplift the body directly from the rest, the rocking conditions around the two adjacent sides of the base have to be simultaneously satisfied. For example, to uplift the body and, consequently, to get 3D motion around the vertex A, rocking conditions around AB and AD have to be satisfied.

When the body is rocking around a side of the base, AB as example, the uplift condition on the vertex A is similar to the one for the 2D rocking motion on the side AD. The overturning moment M_o has to be at least equal to the resisting moment M_r:

$$M_o = ma_{g_x} h'_G = M_r = m\ddot{u}_z(b_x + e_x). \tag{9}$$

In this case, h'_G is the actual height of the center G of the body during a rocking around the x-axis (see Fig. 2$_b$). The quantity h'_G can be evaluated as in [22] by the relation $h'_G = h_G \cos\vartheta_x + (b_y + e_y)\sin\vartheta_x$. By using the nondimesional quantities of Eq. (5), Eq. (9) reads:

$$\frac{\ddot{u}_x}{\ddot{u}_z} = \frac{1+\varepsilon_x}{\lambda_y} \frac{1}{\left(\frac{1+\varepsilon_y}{\lambda_x}\sin\vartheta_x + \cos\vartheta_x\right)} \tag{10}$$

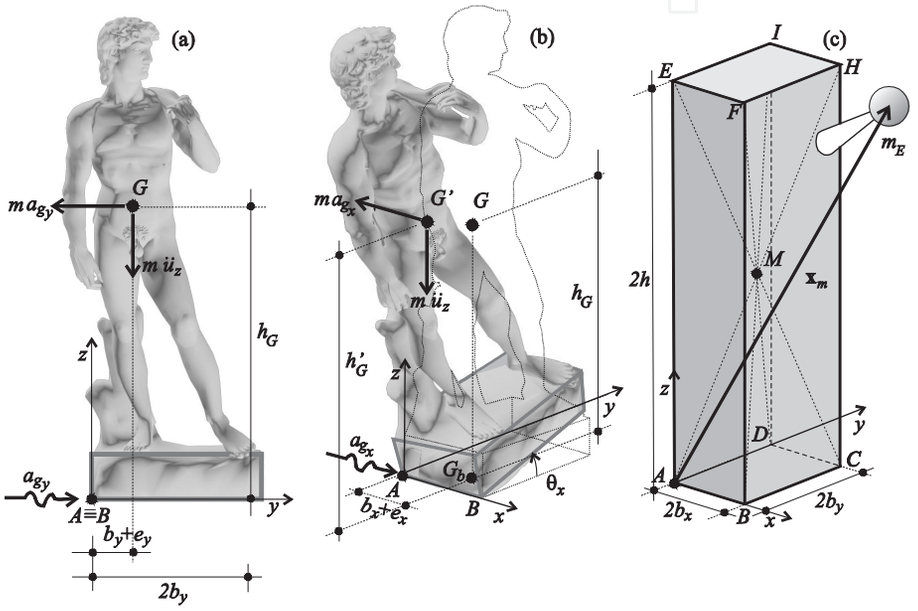

Figure 2. rigid block: (a) forces acting during the full-contact phase; (b) forces acting during a 2D rocking around the AB side; (c) shape of the body used in the numerical simulations.

The natural symmetry of the mechanical system leads to similar conditions for an uplift on one of the other three vertices of the base.

For a square based body with no eccentricity and under an excitation directed along the diagonal, the 3D motion around one of the vertices along the diagonal is directly triggered. This fact highlights how plausible is the occurrence of a 3D rocking motion for a square or near-square based body. An uplift on a vertex could easily manifest itself also in the case of excitation close to the diagonal, just after the occurrence of an uplift on a side and, therefore, during a 2D rocking motion. In fact the vertical position of the center of mass can increase enough ($h'_G > h_G$, see Fig. 2b) to satisfy Eq. (9).

On the contrary, for bodies with rectangular base and a side significantly larger than the other, an overturn around the largest side of the base is much more likely to occur before the uplift on a vertex.

http://dx.doi.org/10.5772/54863

3.2.3. Rocking termination and collapse conditions

No particular conditions are assumed to describe the termination of the motion and the return to the full-contact phase. This means that the rocking motion finishes when the energy associated to this phase is completely dissipated. A collapse event occurs when the body overturns. In the analyses, this condition conventionally manifests itself when one of the four upper vertices of the parallelepiped containing the body hits the ground.

3.3. Impact conditions

The impact conditions are taken from [29] too. They model the process of changing of the vertex around which the rocking occurs, and take place when the base of the block hits the ideal, horizontal, coordinate plane $z=0$. Positions of the body underneath this plane are not allowed. For instance, if the body is rocking around the vertex i ($i=A, B, C, D$) and, at some special time t, another vertex, say j ($j\neq i$), hits the horizontal plane, then the impact process happens and j becomes the new center or rotation. The angles just after the impact (instant t^+) are exactly the same than those just before the impact (instant t^-): $\vartheta_1^+(t)=\vartheta_1^-(t)$, $\vartheta_2^+(t)=\vartheta_2^-(t)$, $\vartheta_3^+(t)=\vartheta_3^-(t)$, and therefore $\mathbf{R}^+(t)=\mathbf{R}^-(t)$. On the other hand, the evaluation of the time-derivatives of the three angles after the impact is made by equating the angular momentum around the (new) center of rotation just after and before the impact (see [29], [31]). In particular, the impact conditions read

$$\mathbf{R}^+(t)\hat{\mathbf{J}}_j\mathbf{R}^T(t)=\mathbf{R}^-(t)\hat{\mathbf{J}}_{ji}\mathbf{R}^T(t) \tag{11}$$

where $\hat{\boldsymbol{J}}_j:=\int_{\hat{C}}\rho(\hat{\mathbf{x}}-\hat{\mathbf{x}}_j)\otimes(\hat{\mathbf{x}}-\hat{\mathbf{x}}_j)dV$ and $\hat{\boldsymbol{J}}_{ji}:=\int_{\hat{C}}\rho(\hat{\mathbf{x}}-\hat{\mathbf{x}}_j)\otimes(\hat{\mathbf{x}}-\hat{\mathbf{x}}_i)dV$ are (initial) Euler tensors. Equations (11) provide a linear non-homogeneous algebraic system in the unknowns $\vartheta_1^+(t)$, $\vartheta_2^+(t)$ and $\vartheta_3^+(t)$, in terms of $\vartheta_1^-(t)$, $\vartheta_2^-(t)$ and $\vartheta_3^-(t)$.

4. Description of the excitations

4.1. One-sine excitation

The three-dimensional rigid body is excited by a one-sine pulse acceleration applied to the base of the body and acting along the horizontal direction ($a_h(t)$) or both along the horizontal and the vertical directions ($a_h(t)$, $a_v(t)$). The analyses are performed by varying the direction of the horizontal excitation, the period of the sine-pulses and their amplitudes. The direction is measured by a counterclockwise angle starting from the x-axis. The pulse-type acceleration used in the analyses are

$$\begin{cases} a_h(t) = A_h \sin\left(\dfrac{2\pi}{T_h} t\right) & 0 \le t \le T_h \\ a_h(t)=0 & T_h < t \le t_{\max} \\ a_v(t) = -A_v \sin\left(\dfrac{2\pi}{T_v} t + \phi\right) & 0 \le t \le T_v \\ a_v(t)=0 & T_v < t \le t_{\max} \end{cases} \tag{12}$$

where h and v stand for horizontal and vertical, respectively; T_h and T_v are the periods of the two one-sine pulses, A_h and A_v are their amplitudes and $T_{\max}$ is the maximum time used in the numerical integrations. This is always taken at least five times the period T_h. The phase of the one-sine horizontal excitation is assumed always equal to zero in this paper, although this parameter, in principle, can affect the behavior of the system. Only the phase of the vertical excitation will be taken into account, since the objective of the analysis is to point out the role of the difference of phase between the horizontal and vertical sine pulses.

4.2. Seismic excitation

In the seismic analysis, only the horizontal effects of the seismic source $\ddot{u}_g = \gamma f(t)$ are considered, where $f(t)$ is the registered seismic acceleration normalized to a $PGA = 1\ g$ (PGA stands for Peak Groung Acceleration) and γ is a variable coefficient used to scale the amplitude of the seismic accelerations. The time-histories and the elastic response spectrums of the three normalized seismic inputs used in the analyses are shown in Fig. 3. Brienza, Buia and Calitri earthquakes are choosen with the aim to perform a simplified analysis, able to evaluate the influence of the spectral characteristic of the earthquake in the dynamics of the three-dimensional rigid block.

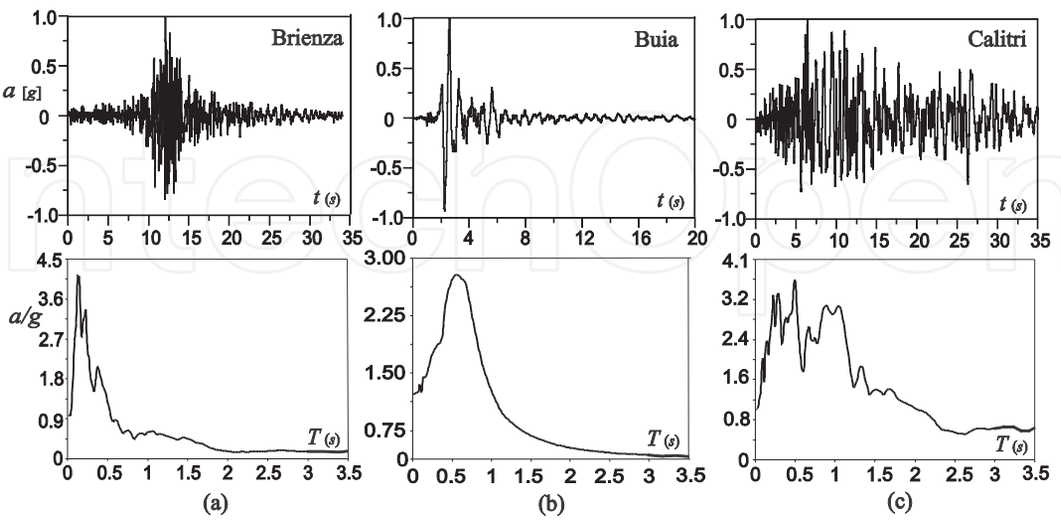

Figure 3. Normalized time-history and spectrum of the registered Italian earthquakes used in the numerical simulations: (a) Brienza earthquake ($PGA = 2.2\ m/s^2$, $lenght = 34.012\ s$); (b) Buia earthquake ($PGA = 2.3\ m/s^2$, $lenght = 20.252\ s$); (c) Calitri earthquake ($PGA = 1.2\ m/s^2$, $lenght = 35.019\ s$).

http://dx.doi.org/10.5772/54863

4.3. Description of the simulation

Results have been obtained by the numerical integration of the equations of motion. A Fortran code has been implemented by using the IMSL Math libraries [30]. In particular the DASPG routine, able to numerically integrate the equations of motion in implicit form, has been chosen. It uses the well known Gear's Backward-Differentiation-Formulas method. Special care has been devoted to the detection of impacts. The integration time step has been fixed for all the simulation to $1/2^{16}$ sec. At each integration step, checks are made in order to verify if, under vertical excitation, the conditions of sliding or free-flight occur. Consequently the results of the evaluation have not been taken into account, since the model is not able to describe them.

For the one-sine excitation, the analyses are conducted by varying continuously the direction of the horizontal excitation and by evaluating the amplitudes of the horizontal or vertical one-sine pulse at which an uplift or an overturning collapse event manifests itself. This type of analysis is performed for several values of other parameters, such as period of the excitations, phase between the horizontal and vertical pulses, eccentricity and geometrical characteristics of the body.

The seisimic analyses are performed by exciting rigid blocks with different mechanical and geometrical characteristics, by three different Italian registered earthquakes acting along different directions. Two type of analyses are performed in this study: the first is conducted with the aim to point out if for some directions of the escitation the 3D model of rigid block furnishes more accurate results than the classical 2D models; the other is performed by fixing the direction of the input, with the aim to highlight the role of the mechanical and the geometrical characteristics of the rigid block in the seismic response.

In the following analyses, a rigid body in the shape of a parallelepiped with a volume equal to $V=8(b_x b_y h)$ is always assumed. The eccentricity of the mass center with respect to the geometrical center of the parallelepiped, when considered, is obtained by introducing a concentrated mass $m_E=\beta m$ and, however, always keeping the total mass m of the body constant (Fig. 2c). This means that the mass of the body with eccentricity $m=\bar{\rho}V(1+\beta)$ is taken equal to the mass of the body without eccentricity $m=\rho V$. As a consequence the mass density $\bar{\rho}$ of a body when an eccentricity is considered leads to $\bar{\rho}=\frac{\rho}{1+\beta}$. The value of $\beta=0.20$ and $\rho=2000 kg/m^3$ are always taken in the following analyses.

5. Description of the results

Results are shown by using polar diagrams where, along the angle-axis (external circle), the angle that measures the direction of the horizontal excitation with respect to the x-axis, positive if counterclockwise, is reported. Along the radial-axis, the amplitude of the horizontal or vertical excitation able to uplift or to overturn the body is reported. These diagrams have been obtained by a massive use of calculator. Increments equal to 1.0^o for the direction of the pulse and equal to $0.01g$ for the amplitudes have been adopted to

obtain the following diagrams. To give an idea of the calculus time needed to get all the results, from which those shown in this paper have been selected, a calculator with 12 Gb ofRAM and a Intel-I7 quad-core CPU with 2.0 GHz clock has been running for about two months.

In the following figures (Figs. 4, 5, 7-13), the same line styles are used. Solid thick lines refer to overturning events (they furnish the amplitude of the excitation at which the first occurrence of an overturning event manifests itself for a specific direction of the pulse). Dashed thick lines refer to the uplift of the body on a side of the rectangular base. In particular, for a specific direction of the excitation, below this curves, the body remains in perfect contact with the ground (full-contact) whereas, above them, a 2D rocking motion occurs. Dotted curves furnish the amplitude of the excitation for which an uplift on a vertex of the base occurs. Above this amplitude, a 3D rocking motion takes place. Directions of the excitation where the body manifests an uplift directly on a vertex (where dashed and dotted curves touch each others) always exist. The analyses performed in this paper do not permit to obtain the so-called survival regions, that could exist also in 3D rocking motions above the first overturning occurrence, as found for 2D rocking motions (see [6, 11]).

5.1. Rocking motion due to one-sine excitation

5.1.1. Rigid block with square base and no eccentricity

The first analysis, shown in Fig. 4, is conducted with the aim to check the influence of the phase ϕ of the one-sine vertical excitation. These results refer to a body with a square base and without any eccentricity of the center of mass, excited by a vertical pulse with fixed amplitude, when considered, and by a horizontal excitation with variable amplitude. The curves reported in the diagrams represent the value of the horizontal amplitude that causes the uplift or the overturning of the body. The angular sectors where a 3D rocking motion manifests itself are marked along the angular circle with solid thick lines. The diagrams shown in Fig. 4_a refer to the case in absence of vertical excitation. It is a case already reported and discussed in [29]. When a vertical one-sine pulse is added to the system, the uplift and overturning curves change as shown in Figs. $4_{b\text{-}d}$.

In particular when $\phi = 90^o$ (Fig. 4b) the sectors where a 3D rocking motion occurs are wider, the system uplifts for smaller horizontal amplitudes and overturns for higher amplitudes (gray curve represents the results reported in Fig. 4_a in absence of vertical pulse). Therefore, with respect to the overturning collapse events, in this case, the presence of the one-sine pulse with this specific phase acts in favor of safety. A change of the phase ($\phi = 180^o$, see Fig. 4_c) produces a worsening of the situation in terms of overturning events. Many angular sectors, where a smaller horizontal amplitude is required to overturn the body, appear; they are contained in 2D or 3D rocking regions. When the phase is $\phi = 270^o$ (Fig. 4_d) the amplitudes necessary to overturn the body become smaller than those obtained in absence of vertical excitation (gray curve) in almost all the angular space.

http://dx.doi.org/10.5772/54863

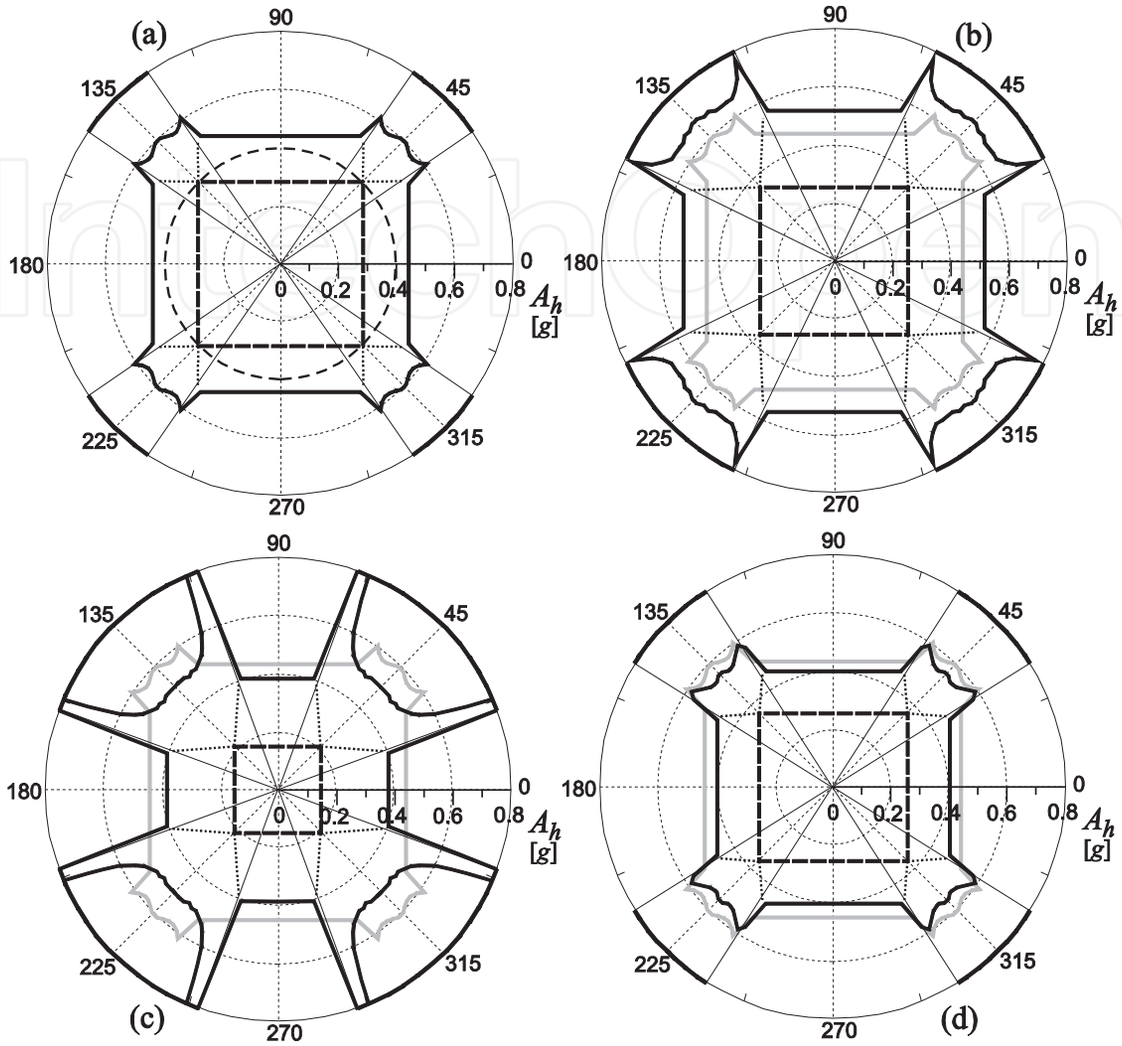

Figure 4. Direction vs Horizontal Amplitude of the excitation: (a) $A_V=0$;(b) $A_V=0.5g$, $\phi=90^o$; (c) $A_V=0.5g$, $\phi=180^o$; (d) $A_V=0.5g$, $\phi=270^o$; ($T_h=0.75s$, $T_v=0.75s$, $b_x=b_y=0.3m$, $h=1.0m$, $\varepsilon_x=\varepsilon_y=0$).

With respect to the previous case, results shown in Fig. 5 refer to different periods of the excitations. In Fig. 5_a, the case in absence of vertical excitation is shown ([29]). When a vertical excitation with fixed amplitude and $\phi=0$ is considered (Fig. 5_b), the uplift and the overturning curves strongly change. In particular, in many angular sectors, the horizontal amplitude able to overturn the body becomes smaller than the one in absence of vertical pulse (gray curve). Also a very critical condition takes place: in the gray angular sectors, contained into the 3D rocking regions, the horizontal amplitudes able to overturn the body become smaller than those obtained along the directions 0, 90, 180, 270 degrees, where the excitation is orthogonal to one of the four sides of the base (dash-dot circle). Since, in order to obtain the amplitudes along the directions 0, 90, 180, 270 degrees, a bi-dimensional model of rigid block is sufficient, the necessity to use a 3D model of rigid block to remain in favour of safety, is confirmed.

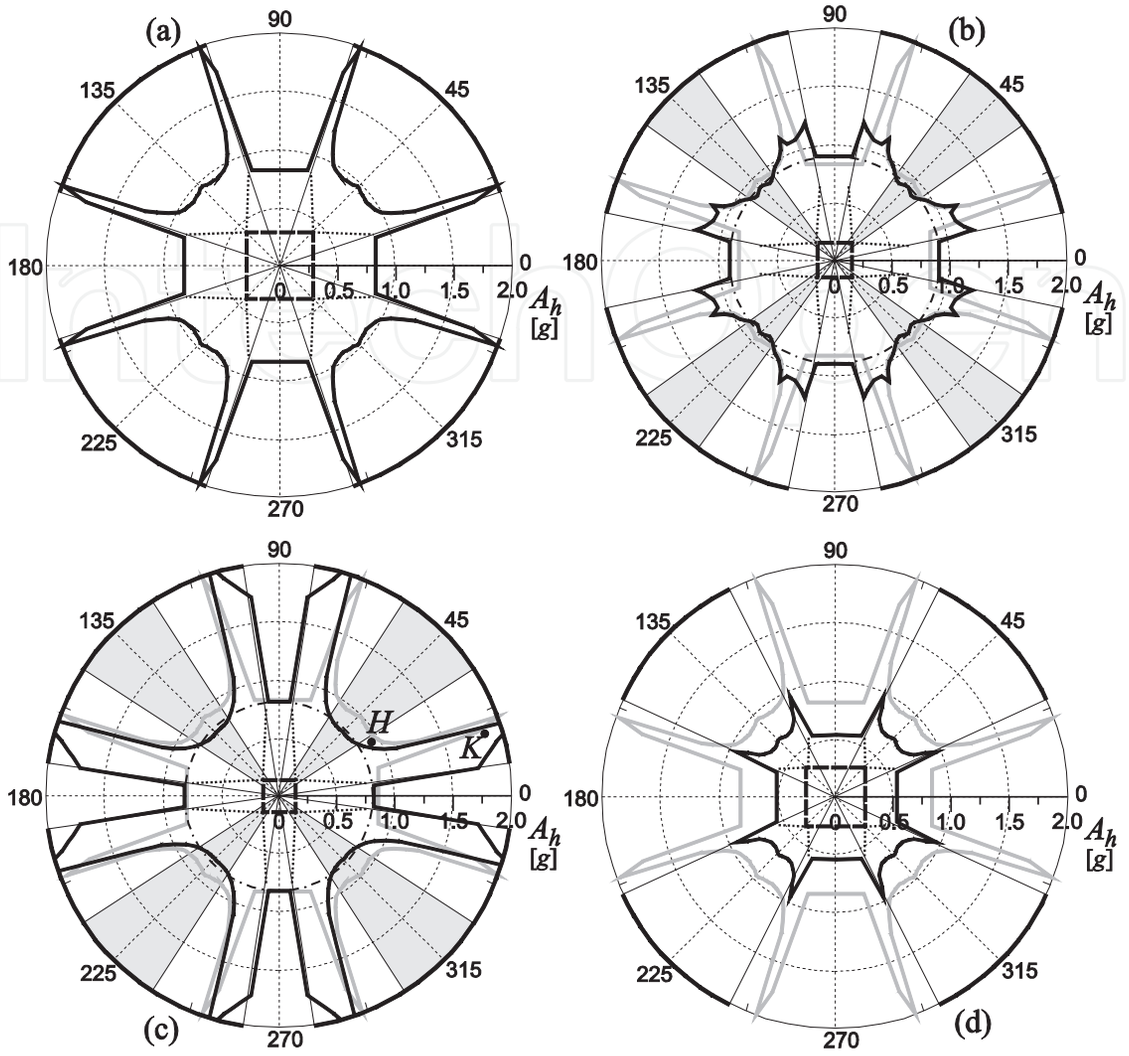

Figure 5. Direction vs Horizontal Amplitude of the excitation: (a) $A_v = 0$;(b) $A_v = 0.5g$, $\phi = 0^o$; (c) $A_v = 0.5g$, $\phi = 180^o$; (d) $A_v = 0.5g$, $\phi = 270^o$; ($T_h = 0.5s$, $T_v = 0.5s$, $b_x = b_y = 0.3m$, $h = 1.0m$, $\varepsilon_x = \varepsilon_y = 0$).

It is interesting to note that the case in absence of vertical excitation (Fig. 5_a) does not manifest the necessity of the use of a 3D model. Therefore, it is possible to assert that this critical situation is only caused by the presence of vertical excitation. A change of the phase of the vertical pulse ($\phi = 180^o$, see Fig. 5_c) causes the enlargement of the critical sector where the amplitudes obtained by a 3D model are smaller than the amplitude of a 2D model (dash-dot circle). A further change of the phase ($\phi = 270^o$, see Fig. 5_d) strongly changes the scenario. The critical gray sectors disappear whereas, in all the angular plane, the overturning amplitudes become smaller than the case in absence of vertical excitation (gray curve).

In Fig. 6 the time-histories of vertical position zA of the base point A and of the angle ϑ_y, referring to the cases labeled with H and K in Fig. 5_c, are shown. Point H refers to a case where, in absence of vertical pulse, the body does not overturn whereas, when the vertical excitation is considered, the body does overturn (Fig. 6_a); point K refers to a case where, in absence of

http://dx.doi.org/10.5772/54863

vertical pulse, the body overturns whereas, when the vertical excitation is considered, the body does not overturn (Fig. 6_b). Solid curves represent the case with vertical excitation, whereas dashed curves the case without vertical excitation. In both cases, where the body does not overturn, the time-histories zA touch and remain on the $zA=0$ axis in several time ranges. This happens when, during the 3D rocking motion, the point A hits the ground and becomes the instantaneous rotation center.

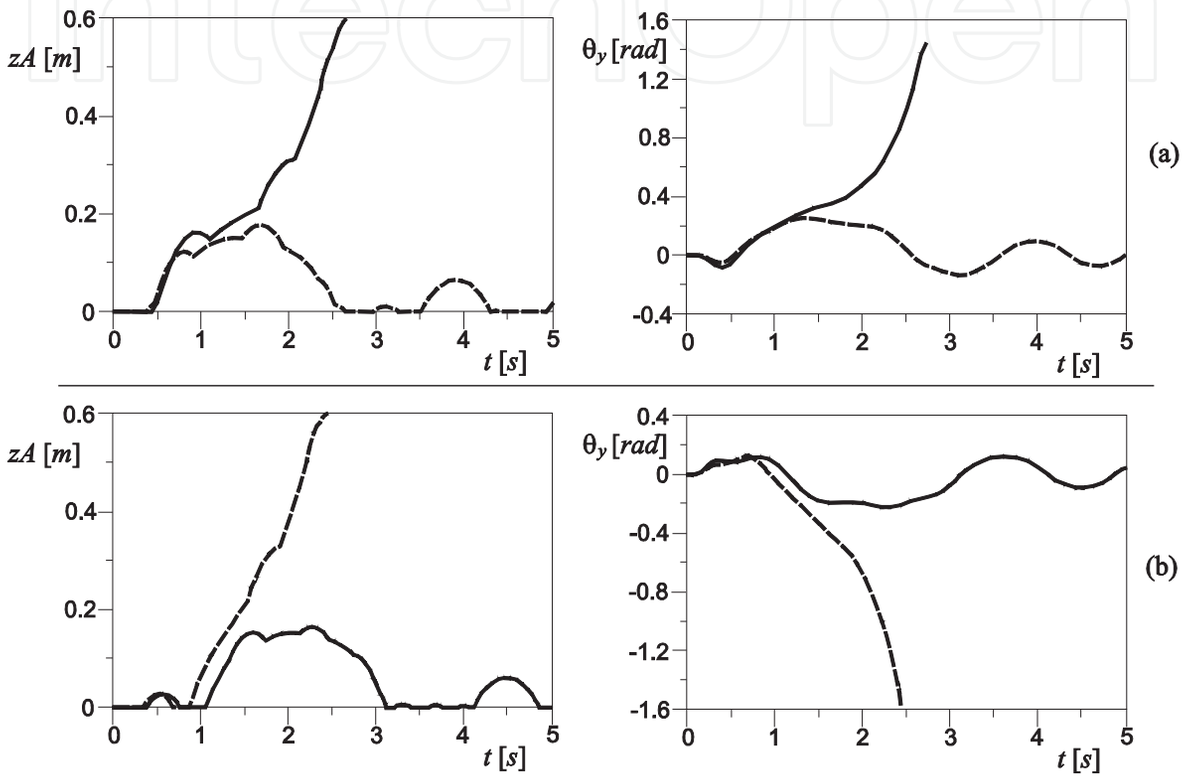

Figure 6. Time-histories: (a) Vertical position of the vertex A and angle $_y$ vs time calculated at point H labeled in Fig. 5c ($A_h=0,875g$, $A_v=0.5g$, $\alpha=30^o$, $\phi=180^o$); (b) Vertical position of the vertex A and angle $_y$vs time calculated at point K labeled in Fig. 5c ($A_h=1.74g$, $A_v=0.5g$, $\alpha=18^o$, $\phi=180^o$); ($T_h=0.5s$, $T_v=0.5s$, $b_x=b_y=0.3m$, $h=1.0m$, $\varepsilon_x=\varepsilon_y=0$;solid lines: with vertical excitation, dashed lines: without vertical excitation).

Very interesting is the case shown in Fig. 7. The results refer to a value of the period of the horizontal one-sine pulse for which, in absence of vertical excitation, many sectors where the 3D model furnishes more accurate results with respect to the classical 2D model exist (gray sectors in Fig. 7_a, see [29] for more details). The vertical excitation, also in this case, strongly changes the scenario. In particular, when the $\phi=0$ (Fig. 7_b), the critical gray sectors reduce but, in all the angular plane, the overturning amplitudes become smaller than those obtained without vertical pulse (gray curve). For $\phi=90^o$ (Fig. 7_c) in several angular sectors the amplitude able to overturn the body becomes higher than the one obtained without vertical excitation, but the critical gray sectors, where it is necessary the use of a 3D model to better evaluate the overturning of the body, completely disappear. These critical regions appear again for $\phi=180^o$

(Fig. 7_d) but the overturning amplitudes become higher than those obtained in absence of vertical pulse, in all the angular plane.

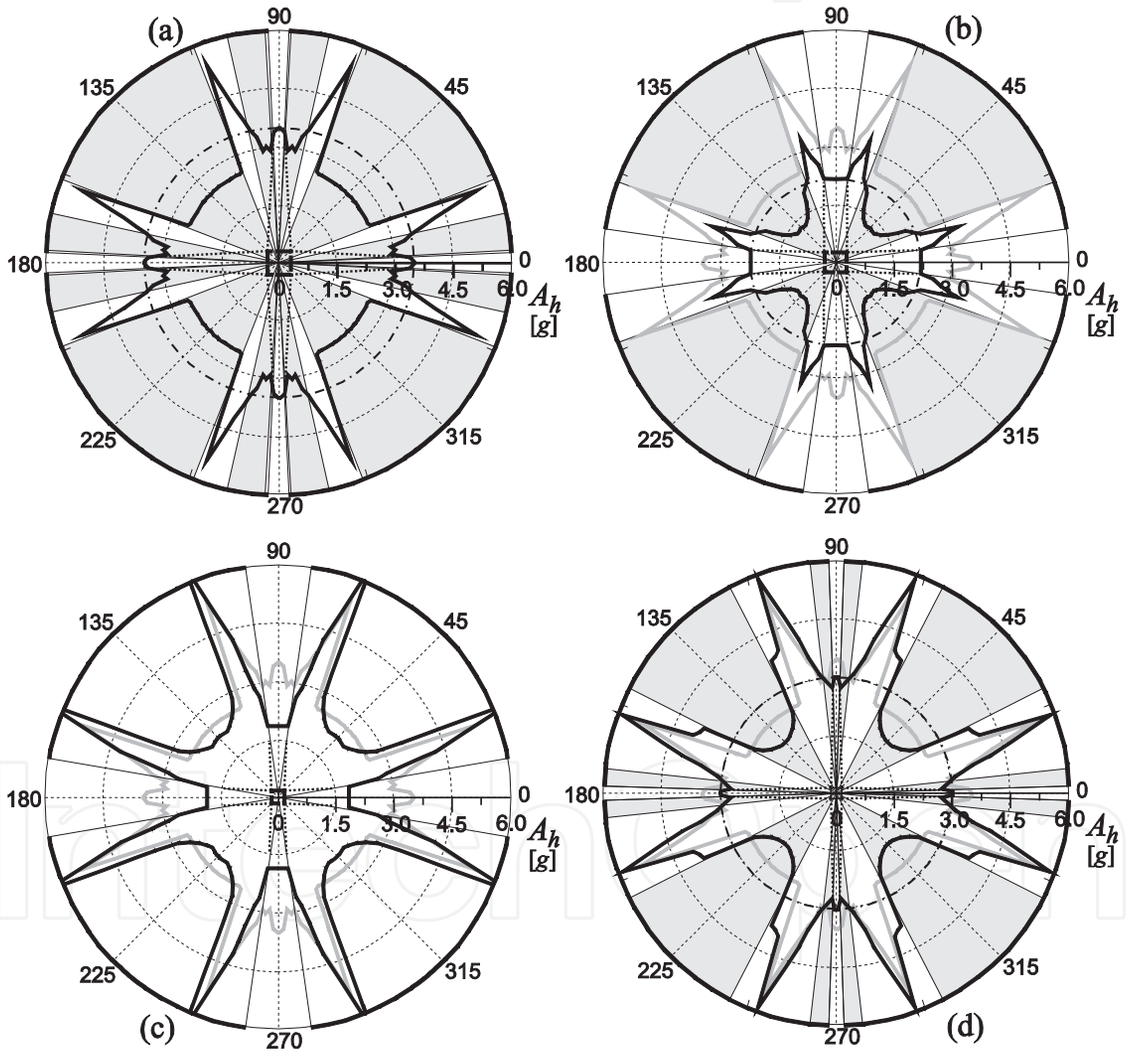

Figure 7. Direction vs Horizontal Amplitude of the excitation: (a) $A_v=0$;(b) $A_v=0.5g$, $\phi=0^o$; (c) $A_v=0.5g$, $\phi=90^o$; (d) $A_v=0.5g$, $\phi=180^o$; ($T_h=0.35s$, $T_v=0.5s$, $b_x=b_y=0.3m$, $h=1.0m$, $\varepsilon_x=\varepsilon_y=0$).

http://dx.doi.org/10.5772/54863

5.1.2. Rigid block with square base and with eccentricity

In Fig. 8 the role of a fixed vertical excitation applied to a square based, eccentric, rigid body is investigated. The case of absence of vertical excitation, horizontal pulse with period $T_h = 0.75s$ and eccentricities $\varepsilon_x = \varepsilon_y = 0.25$, is shown in Fig. 8_a (see [29] for more details). Two critical regions (gray sectors) where a 3D model is necessary to better evaluate the overturning collapse events manifest themselves. When a vertical fixed excitation is considered, a change of the previous scenario occurs. In particular, for $\phi = 0$ and $\phi = 270^o$ (Fig. 8_b and 8_d respectively), a slightly modification of the critical sectors takes place: A diminution of the horizontal overturning amplitude with respect to the case in absence of vertical pulse (gray curve) manifests itself. For $\phi = 90^o$ (Fig. 8_c), the critical regions disappear.

5.1.3. Rigid block with near-square base

Finally, in Fig. 9, the role of a fixed vertical excitation applied to a near-square based, eccentric, rigid body is investigated. The case of absence of vertical excitation, without and with eccentricity ($\varepsilon_x = 0$, $\varepsilon = 0.5$) are shown in Fig. 9_a and Fig. 9_b, respectively (see [29] for more details). The eccentricity of the mass center of the body is the cause of the apparition of the critical regions (gray sectors, Fig. 9_b) where the overturning amplitude obtained during a 3D rocking motion is smaller than the overturning amplitude furnished by a 2D model (dash-dot circle). The vertical excitation, in addition to changing the overturning curves, acts also on thecritical regions. In particular, for $\phi = 0$ (Fig. 9_c), two new critical regions appear whereas, for $\phi = 90^o$ (Fig. 9_d), these critical regions change their position and amplitude with respect to the case where the vertical excitation is null (Fig. 9_b).

5.2. Rocking motion due to seismic excitation

5.2.1. The role of the direction of the input

In the first analysis, square based block with constant height are excited by the three different earthquakes. In particular results reported in Fig. $10_{a,b}$ refer to two different blocks ($30 \times 30 \times 200$ cm^3 and $50 \times 50 \times 200 cm^3$, respectively) subject to the Brienza earthquake. It is possible to observe a general increase of the PGA able to overturn the body when the dimension of the base increases. Also a slight increase of the sectors of 3D rocking motion manifests itself for higher bases of the block. The overturning amplitude in 3D regions is always larger than the amplitude able to overturn the body during a 2D rocking motion (the value observed along the 0^o, 90^o, 180^o, 270^odirections) and marked in the graphs with a dash-dotted circle. However, for larger bases of the body, the 3D overturning amplitude becomes very close to the 2D overturning PGA, along some specific directions of the excitation. A similar behavior can be observed when the same previous blocks are excited by the Buia earthquake (Fig. $10_{c,d}$). Very different are the results obtained by exciting the body by the Calitri earthquake (Fig. $10_{e,f}$). The amplitude of the sectors where a 3D rocking motion manifests itself are a lot smaller than the previous cases and the 3D overturning amplitude remains always far enough from the 2D overturning PGA (dash-dotted circle). However, smaller values of the PGA than the previous earth-

quakes are requested to cause a collapse event. Considering the results of these first analyses, it does not seem necessary the use of a 3D model to study the seismic behavior of a rigid block, since the most dangerous situations manifest themselves during a 2D rocking motion.

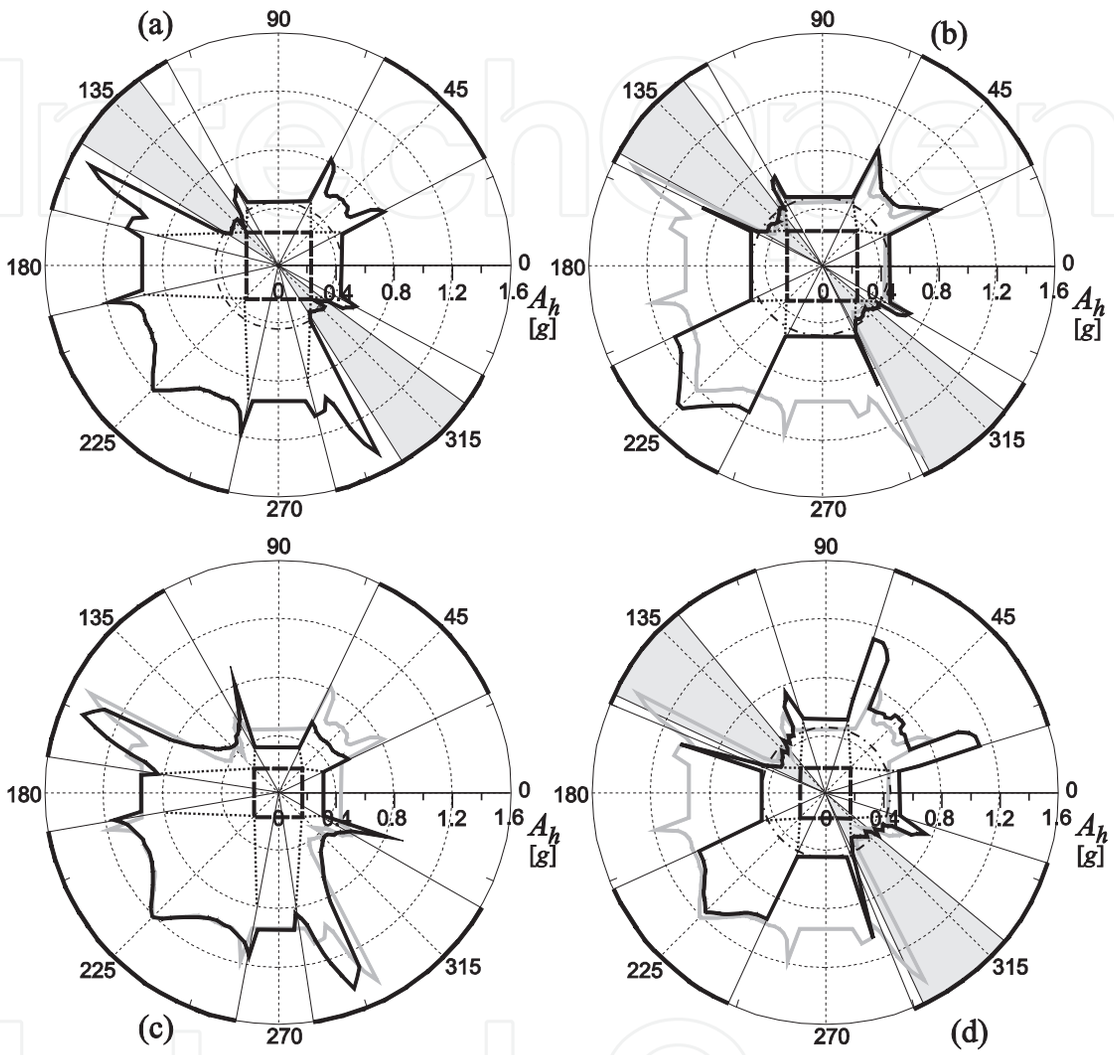

Figure 8. Direction vs Horizontal Amplitude of the excitation: (a)$A_v=0$; (b) $A_v=0.5g$, $\phi=0^o$; (c) $A_v=0.5g$, $\phi=90^o$; (d) $A_v=0.5g$, $\phi=270^o$; ($T_h=0.75s$, $T_v=0.5s$, $b_x=b_y=0.3m$, $h=1.0m$,$\varepsilon_x=\varepsilon_y=0.25$).

In Fig. 11 the effect of the eccentricity of the mass center is outlined. In particular, a block of dimensions $40\times40\times200cm^3$, with and without eccentricity, is excited by the three different earthquakes. Results shown in Fig. $12_{a,b}$ refer to the case without eccentricity and the case with eccentricity along the y-axis ($\varepsilon_y=0.25$, $e_y=5$ cm) respectively. The presence of an eccentricity sensibly changes the overturning curve, that loses one symmetry axis and becomes more irregular than the case without eccentricity.

However, a very interesting phenomenon occurs in presence of the eccenticity: in some directions inside the 3D rocking regions (marked with thick lines along the external circle),

http://dx.doi.org/10.5772/54863

overturnig PGA's smaller than the minimum required during the 2D rocking motion (dash-dotted circle) manifest themselves. In other words, inside the gray sectors, during a 3D rocking motion, an overturning collapse event occurs for a PGA smaller than the minimum obtained by using a 2D model of rigid block. Results shown in Fig. $11_{c,d}$, that refer to Buia earthquake, confirm what previously said. The situation changes if the block is excited by the Calitri earthquake (Fig. $11_{e,f}$). In this case the 3D overturning amplitudes remain always far enough from the 2D overturning PGA's, also when an eccentricity is considered.

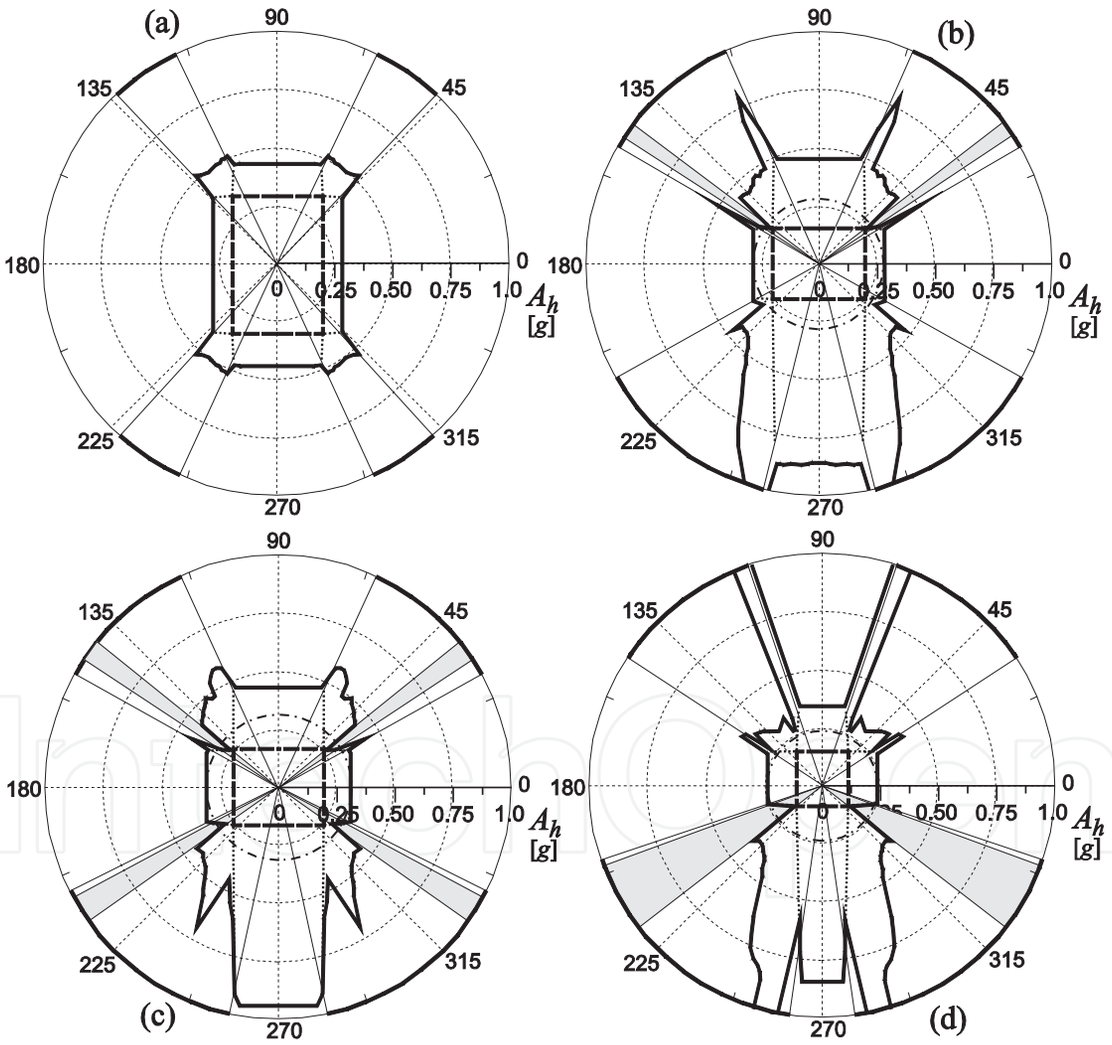

Figure 9. Direction vs Horizontal Amplitude of the excitation: (a) $A_v=0$, $\varepsilon_x=\varepsilon_y=0$; (b) $A_v=0$, $\varepsilon_x=0$, $\varepsilon_y=0.5$; (c) $A_v=0.5g$, $\varepsilon_x=0$, $\varepsilon_y=0.5$, $\phi=0^o$; (d) $A_v=0.5g$, $\varepsilon_x=0$, $\varepsilon_y=0.5$, $\phi=0^o$; ($T_h=0.75s$, $T_v=0.5s$, $b_x=b_y=0.3m$, $h=1.0m$).

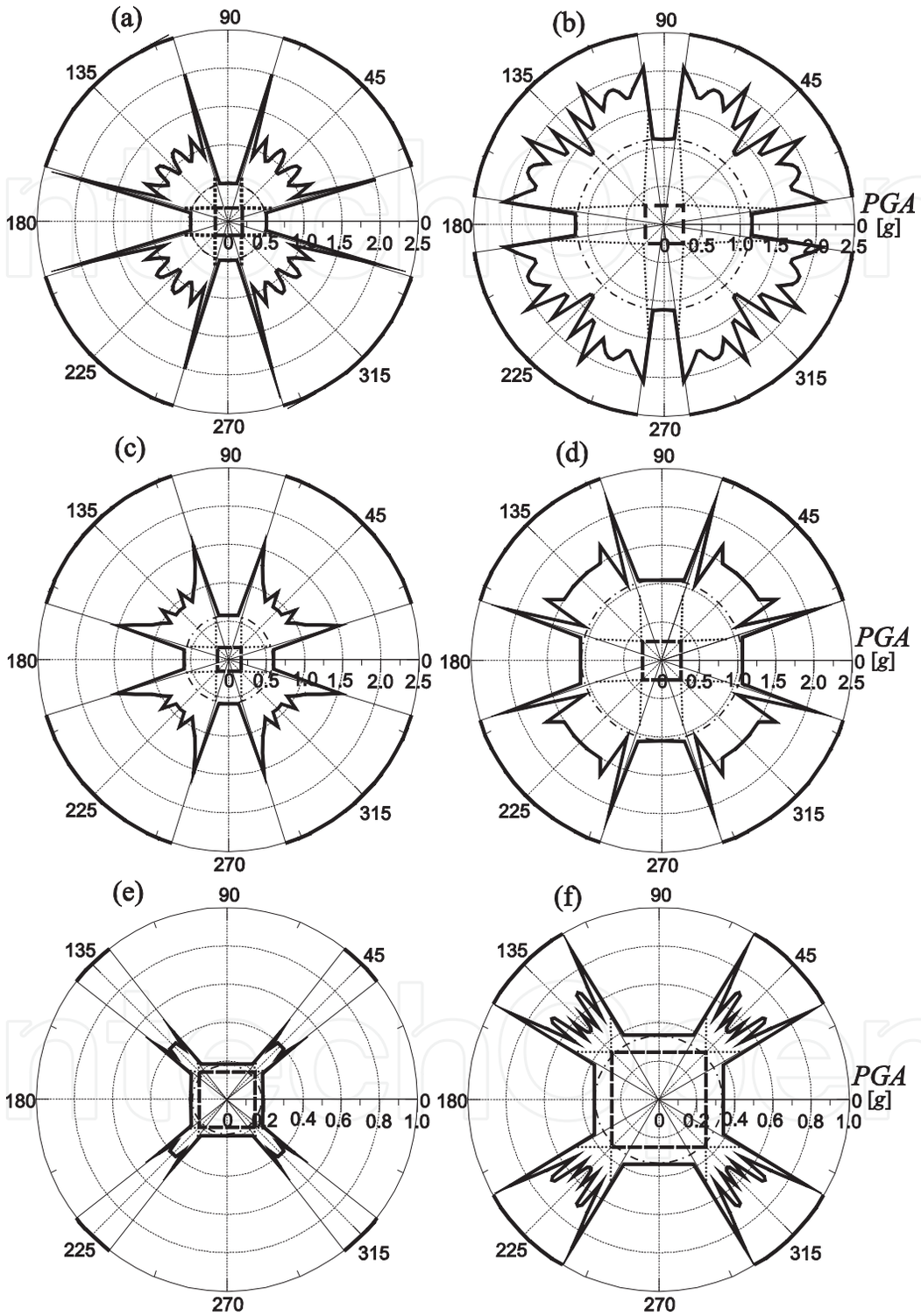

Figure 10. Direction vs Amplitude of the excitation. Brienza earthquake: (a)$30\times30\times200$; (b) $50\times50\times200cm^3$. Buia earthquake: (c)$30\times30\times200$; (d) $50\times50\times200cm^3$. Calitri earthquake: (e)$30\times30\times200$; (f) $50\times50\times200cm^3$,($\varepsilon_x=\varepsilon_y=0$).

http://dx.doi.org/10.5772/54863

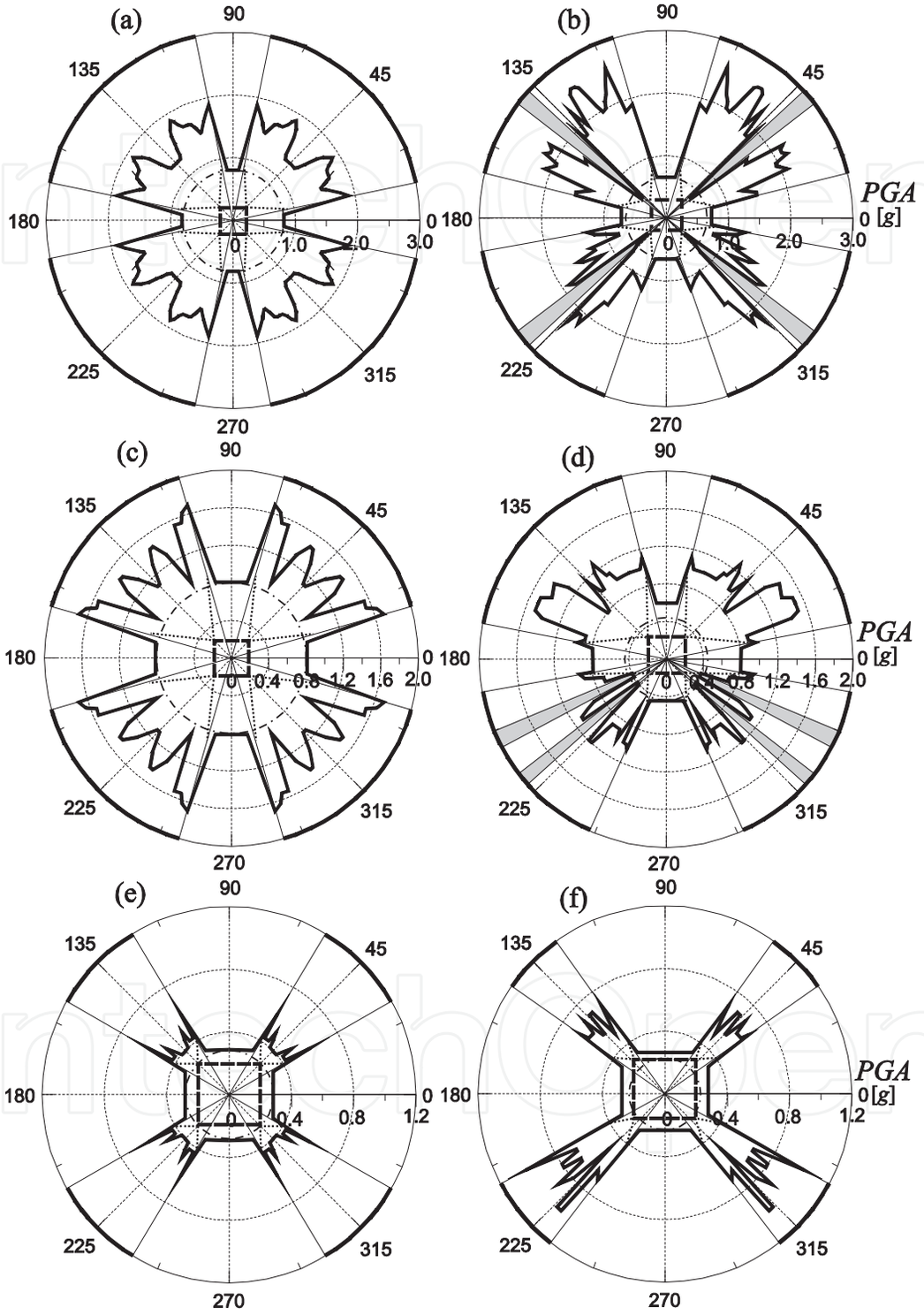

Figure 11. Direction vs Amplitude of the excitation. Brienza earthquake: (a)$\varepsilon_x = \varepsilon_y = 0$; (b)$\varepsilon_x = 0$, $\varepsilon_y = 0.25$. Buia earthquake: (c)$\varepsilon_x = \varepsilon_y = 0$; (d)$\varepsilon_x = 0$, $\varepsilon_y = 0.25$. Calitri earthquake: (e)$\varepsilon_x = \varepsilon_y = 0$; (f) $\varepsilon_x = 0$, $\varepsilon_y = 0.25$ $(40 \times 40 \times 200) cm^3$.

To summarize, when the block is excited by an earthquake with narrow spectrum (Brienza and Buia earthquakes, see Fig. $3_{a,b}$), the presence of a small eccentricity makes possible the existence of angular sectors inside the 3D rocking regions, where the use of the 3D model of rigid block is necessary to obtain results in favour of safety. On the contrary, a wide spectrum earthquake (Calitri earthquake, see Fig. 3_c) does not require the use of the 3D model of rigid block, since the eccentricity of the mass center never causes the existence of these critical sectors inside the 3D rocking regions.

Finally, the case of blocks with a rectangular base is considered. Results shown in Fig. $12_{a,b}$ refer to rectangular based block ($30\times40\times200cm^3$), subject to Brienza earthquake, without and with eccentricity ($\varepsilon_x=0,\ \varepsilon_y=0.25$), respectively.

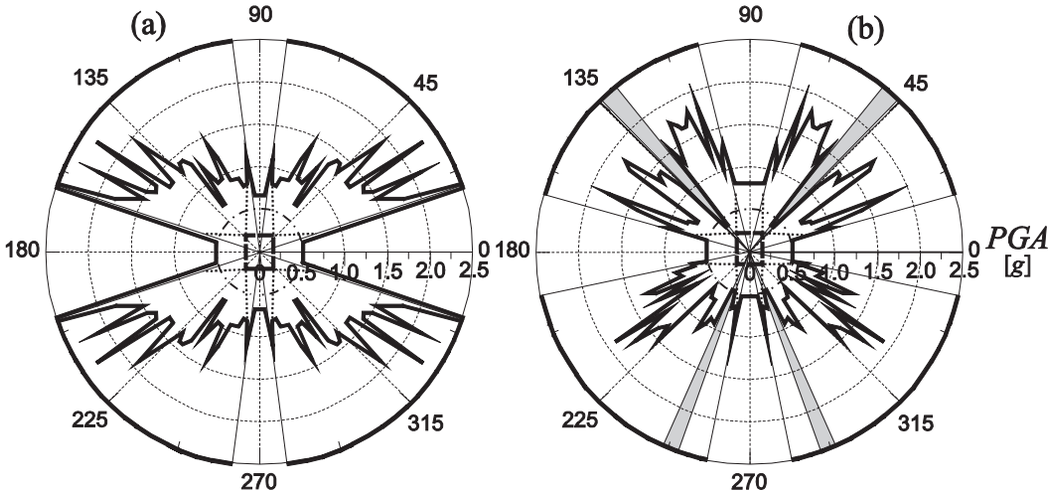

Figure 12. Direction vs Amplitude of the excitation. Brienza earthquake: (a) $\varepsilon_x=\varepsilon_y=0$; (b) $\varepsilon_x=0,\ \varepsilon_y=0.25\,(30\times40\times200)cm^3$.

As it is possible to observe, also in blocks with rectangular base, subject to a narrow spectrum earthquake (Brienza), sectors inside 3D rocking regions where the overturnig PGA's are smaller than the minimum required during the 2D rocking appears. This case is very interesting since, when a rectangular base of a rigid body occurs, the rocking motion is usually analysed by a 2D model in the plane of the smaller dimension of the base. As a consequence, the eccentricity of the mass center in the direction orthogonal to the plane of the analyzed motion is not taken into account. These results highlight the fact that also in this case, to evaluate the behavior of the system in favour of safety, it is necessary the use a 3D model of rigid body.

5.2.2. The role of the mechanical and geometrical characteristics of the body

In this section the analyses are performed by fixing the direction of the excitation and varying other geometrical and mechanical characteristic of the block, to point out their role in the seismic response of a square based body. In particular a first analysis is conducted by fixing the slenderness of the body and varying the base of the body (i.e. varying the volume of the

http://dx.doi.org/10.5772/54863

body); the second analysis is performed by fixing the mass of the body (i.e. fixing the volume of the body) and varying its slenderness. Results of these analyses are reported in Fig. 13. In all the graphs, solid curves refer to PGA able to overturn the body when the excitation angle is $\alpha = 40^o$, while dashed curves refers to overturning events when the excitation angle is $\alpha = 0$. Dotted curves, when reported, refer to overturning amplitude when the direction of the excitation is $\alpha = 40^o$ and in presence of a very small eccentricity ($\varepsilon_x = 0$, $\varepsilon_y = 0.1$). The chosen directions permit to compare the overturning seismic response of the body during the 2D rocking motion ($\alpha = 0$) and the 3D rocking motion ($\alpha = 40^o$).

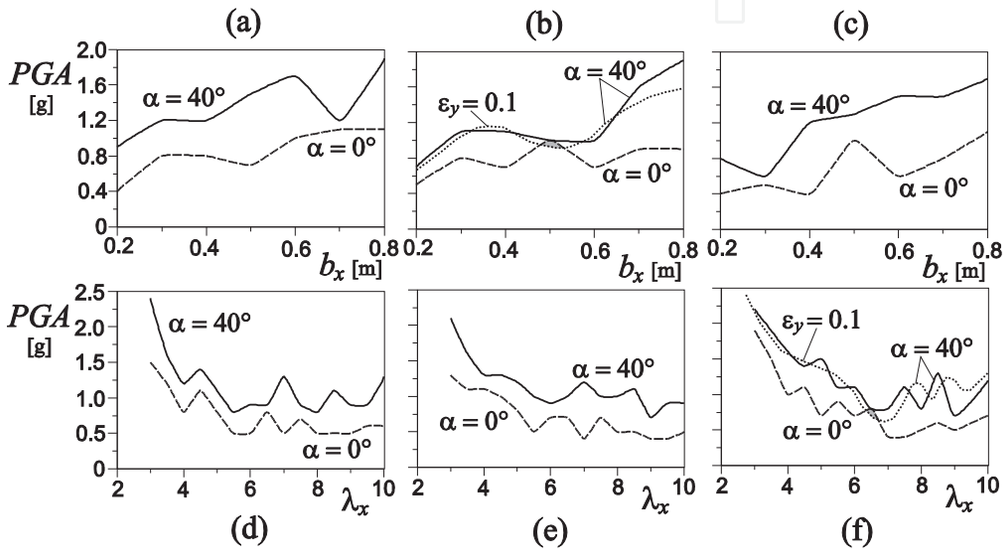

Figure 13. Overturning curves under Brienza earthquake: (a)$\lambda_x = \lambda_y = 5$; (b)$\lambda_x = \lambda_y = 6$; (c)$\lambda_x = \lambda_y = 7$; (d)$m = 500\,kg$; (e) $m = 640\,kg$; (f)$m = 800\,kg$.

The sequence of results shown in Fig. $13_{a\text{-}c}$ refers to cases with fixed slenderness $\lambda_x = \lambda_y = 5,\ 6,\ 7$). As it is possible to observe the two curves (solid and dashed curves) approach to each other at different values of the dimension of the base, depending on the slenderness used in the analysis. An increasing slenderness requires a decreasing base dimension to make possible the approach of the two curves. Very interesting is the case shown in Fig. 13_b ($a_x = \lambda_y = 6$) where the two curves touch each other. For this particular dimension of the base of the block, the same PGA is required to overturn the body during the 2D rocking motion and the 3D rocking motion, when the direction of the excitation is $\alpha = 40^o$. The presence of a small eccentricity changes the 3D overturning curve (dotted curve) by making possible the existence of a region where the overturning PGA during the 3D motion is smaller than the one during the 2D motion. On the contrary, the sequence of results shown in Fig. $13_{d\text{-}f}$ refers to cases with fixed mass ($m = 500,\ 640,\ 800\,kg$). The two curves (solid and dashed curves) approach to each other at different values of the slenderness, depending on the mass of the body used in the analysis. Very interesting is the case shown in Fig. 13_f ($m = 800\,kg$) where the two curves touch each other. Also in this case the presence of a small eccentricity (dotted curve) makes possible

the existence of a region where the overturning PGA during the 3D motion is smaller than the one during the 2D motion.

Finally, when the body is excited by a narrow spectrum earthquake, it is always possible to find cases where a 3D model of rigid block is necessary to evaluate the seimic responce in favour of safety.

6. Conclusion

The rocking motion around a side or a vertex of a rectangular based rigid body has been deeply studied, making use of a three-dimensional model already proposed by the same authors. Starting conditions of motion have been found by means of equilibrium between overturning and resisting moments, whereas the impact has been described considering the conservation of the angular momentum.

The dynamics of the rigid body excited by one-sine pulse horizontal and vertical excitations and horizontal seismic excitation has been analyzed. Rocking and overturning curves versus the angular direction of the horizontal pulse have been obtained. The influence on the motion of several parameters, such as the period of the excitations, the geometrical characteristics of the body and of the eccentricity of the mass center has been pointed out.

The vertical one-sine pulse strongly modifies the behavior of the system with respect to the case where only horizontal excitation acts on the body. Results show that, in presence of vertical excitation and in significant ranges of the parameters, as happens when just horizontal base acceleration is considered, bi-dimensional models are not enough accurate to correctly evaluate the occurrence of the overturning and, therefore, a three-dimensional model is needed.

The seismic response of the rigid body excited by three different Italian registered earthquakes has been analyzed, reporting rocking and overturning curves. Results show that, for narrow spectrum earthquakes, bi-dimensional models are not enough accurate to correctly evaluate the occurrence of the overturning since, in significant sectors inside the 3D rocking regions, the overturning amplitudes are smaller than the ones given by the 2D models. Hence a 3D model of rigid block is necessary to evaluate the seismic response of a rigid block in favour of safety.

Appendix A. Vector and tensor quantities

The rotation $\mathbf{R}$ is the composition of three planar rotations: if $\{\mathbf{e}_x, \mathbf{e}_y, \mathbf{e}_z\}$ is the canonical basis, the first rotation, indicated as $\mathbf{R}_1$, of angle ϑ_1, is around the axis $\mathbf{e}_x$; the second, indicated as $\mathbf{R}_2$, of angle ϑ_2, around the axis $\mathbf{R}_1\mathbf{e}_y$; the third, indicated as $\mathbf{R}_3$, of angle ϑ_3, around the axis $\mathbf{R}_2\mathbf{R}_1\mathbf{e}_z$. The representation of $\mathbf{R}$ on the canonical basis is

http://dx.doi.org/10.5772/54863

$$\left[\mathbf{R}(t)\right]_{\mathbf{e}_{x,y,z}} = \begin{pmatrix} c_2c_3 & s_1s_2c_3 - c_1s_2 & c_1s_2c_3 + s_1s_3 \\ c_2s_3 & c_1c_3 + s_1s_2s_3 & c_1s_2s_3 + s_1c_3 \\ -s_2 & s_1c_2 & c_1c_2 \end{pmatrix} \tag{13}$$

where, for $k = 1, 2, 3$,

$$\begin{aligned} c_k &:= \cos(\vartheta_k(t)) \\ s_k &:= \sin(\vartheta_k(t)) \end{aligned} \tag{14}$$

When the block is a parallelepiped of uniform mass density, with sides of length $2b_x$, $2b_y$, $2h$, respectively, the positions of the base vertices are

$$\begin{aligned} \hat{\mathbf{x}}_A &= 0 \\ \hat{\mathbf{x}}_B &= \hat{\mathbf{x}}_A + 2b_x\mathbf{e}_x \\ \hat{\mathbf{x}}_C &= \hat{\mathbf{x}}_A + 2b_x\mathbf{e}_x + 2b_y\mathbf{e}_y \\ \hat{\mathbf{x}}_D &= \hat{\mathbf{x}}_A + 2b_y\mathbf{e}_y \end{aligned} \tag{15}$$

The mass is $m = 8\rho b_x b_y h$. The static moment with respect to the point A is

$$\hat{\mathbf{s}}_A = m(b_x\mathbf{e}_x + b_y\mathbf{e}_y + h\mathbf{e}_y) \tag{16}$$

The representation of the Euler tensor with respect to the point A is

$$[\hat{\mathbf{J}}_A]_{\mathbf{e}_{x,y,z}} = m\begin{bmatrix} \frac{4}{3}b_x^2 & b_xb_y & b_xh \\ b_xb_y & \frac{4}{3}b_y^2 & b_yh \\ b_xh & b_yh & \frac{4}{3}h^2 \end{bmatrix} \tag{17}$$

To get the generic static moment $\hat{s}_i$ and the generic Euler tensor $\hat{J}_{ji}$, the transport rules read:

$$\begin{aligned} \hat{\mathbf{s}}_i &= \hat{\mathbf{s}}_A + m(\hat{\mathbf{x}}_A - \hat{\mathbf{x}}_i) \\ \hat{\mathbf{J}}_{ji} &= \hat{\mathbf{J}}_A + \hat{\mathbf{s}}_A \otimes (\hat{\mathbf{x}}_A - \hat{\mathbf{x}}_i) + (\hat{\mathbf{x}}_A - \hat{\mathbf{x}}_j) \otimes \hat{\mathbf{s}}_A \\ &\quad + m(\hat{\mathbf{x}}_A - \hat{\mathbf{x}}_j) \otimes (\hat{\mathbf{x}}_A - \hat{\mathbf{x}}_i) \end{aligned} \tag{18}$$

where the tensor product $\otimes$ is defined such that $(\boldsymbol{u} \otimes \boldsymbol{v})\boldsymbol{w} = (\boldsymbol{u} \cdot \boldsymbol{w})\boldsymbol{v}$ for any vectors $\boldsymbol{u}$, $\boldsymbol{v}$, $\boldsymbol{w}$ of the same vector space.

Author details

Alessandro Contento, Daniele Zulli and Angelo Di Egidio

Dipartimento di Ingegneria Civile,Edile-Architettura, Ambientale University of L'Aquila, Italy

References

[1] Shenton H, Jones N. Base excitation of rigid bodies. I: Formulation. Journal of Engineering Mechanics 1991; 117: 2286–2306.

[2] Taniguchi T. Non-linear response analyses of rectangular rigid bodies subjected to horizontal and vertical ground motion. Earthquake Engineering and Structural Dynamics 2002; 31: 1481–1500.

[3] Boroscheck R, Romo D. Overturning criteria for non-anchored non-symmetric rigid bodies. In: Proceeding of the 13th World Conference on Earthquake Engineering, 1-6 August 2004, Vancouver, Canada.

[4] Agbabian M, Masri F, Nigbor R, Ginel W. Seismic damage mitigation concepts for art objects in museum. In: Proceeding of the 9th World Conference on Earthquake Engineering, 1998, Tokyo-Kyoto, Japan.

[5] Zhu Z, Soong T. Toppling fragility of unrestrained equipment. Earthquake Spectra 1998; 14: 695–712.

[6] Zhang J, Makris N. Rocking response of free-standing blocks under cycloidal pulses. Journal of Engineering Mechanics 2001; 127: 473–483.

[7] Makris N, Roussos Y. Rocking response of rigid blocks under near-source ground motions, Géotechnique 2000; 50: 243–262.

[8] Spanos P, Koh A. Rocking of rigid blocks due to harmonic shaking. Journal of Engineering Mechanics 1984; 110: 1627–1642.

[9] Makris N, Zhang J. Rocking response of anchored blocks under pulse-type motions. Journal of Engineering Mechanics 2001; 127: 484–493.

[10] Kounadis A. On the overturning instability of a rectangular rigid block under ground excitation. The Open Mechanics Journa 2010; l4: 43–57.

[11] Purvance M, Anooshehpoor A, Brune J. Freestanding block overturning fragilities: numerical simulation and experimental validation. Earthquake Engineering and Structural Dynamics 2008; 37(5): 791-808.

[12] Spanos P,Roussis P, P N P A. Dynamic analysis of stacked rigid blocks. Soil Dynamics and Earthquake Engineering 2000; 21: 559–578.

[13] Spanos P, Koh A. Harmonic rocking of rigid block on fexible foundation. Journal of Engineering Mechanics 1986; 112: 1165–1181.

[14] Spanos P, Koh A. Analysis of block random rocking. Soil Dynamics and Earthquake Engineering 1986; 5: 178–183.

[15] Lenci S, Rega G. Heteroclinic bifurcations and optimal control in the non linear rocking dynamics of generic and slender rigid blocks. International Journal of Bifurcation and Chaos 2005; 5: 1901–1918.

[16] Lenci S, Rega G. A dynamical systems approach to the overturning of rocking blocks. Chaos, Solitons and Fractals 2006; 28: 527–542.

[17] Lenci S, Rega G. Optimal control and anti-control of the nonlinear dynamics of a rigid block. Philosophical Transactions of the Royal Society A 2006; 364: 2353–2381.

[18] ujita K, Yoshitomi S, Tsuji M, Takewaki I. Critical cross-correlation function of horizontal and vertical ground motions for uplift of rigid block. Engineering Structures 2008; 30: 1199–1213.

[19] Iyengar R, Manohar C. Rocking response of rectangular rigid blocks under random noise base excitations. International Journal of Non-Linear Mechanics 1991; 26: 885–892.

[20] Vestroni F, Di Cintio S.,Base isolation for seismic protection of statues. In: Twelfth World Conference on Earthquake Engineering, 2000, New Zealand.

[21] Caliò I, Marletta M. Passive control of the seismic response of art objects. Engineering Structures 2003; 25: 1009–1018.

[22] Contento A, Di Egidio A. Investigations into the benefts of base isolation for non-symmetric rigid blocks. Earthquake Engineering and Structural Dynamics 2009; 38: 849–866.

[23] Di Egidio A,Contento A. Base isolation of sliding-rocking non-symmetyric rigid blocks subjected to impulsive and seismic excitations. Engineering Structures 2009; 31: 2723–2734.

[24] Di Egidio A,Contento A. Seismic response of a non-symmetric rigid block on a constrained oscillating base. Engineering Structures 2010; 32: 3028–3039.

[25] Koh A, Mustafa G. Free rocking of cylindrical structures. Journal of Engineering Mechanics 1990; 116: 34–54.

[26] Batista M. Steady motion of a rigid disc of finite thickness on a horizontal plane. Journal of Nonlinear Mechanics 2006; 41: 850–859.

[27] Stefanou I, Vardoulakis I, Mavraganis A. Dynamic motion of a conical frustum over a rough horizontal plane. International Journal of Nonlinear Mechanics 2011; 46: 114–124.

[28] Taniguchi T. Rocking behavior of unanchored fat-bottom cylindrical shell tanks under action of horizontal base excitation. Engineering Structures 2004; 26: 415–426.

[29] Zulli D, Contento A, Di Egidio A. Three-dimensional model of rigid block with a rectangular base subject to pulse-type excitation. International Journal of Non-Linear Mechanics 2012; 47(6): 679-687.

[30] IMSL Fortran Library User's Guide, Visual Numerics, 2003.

[31] Housner G.The behaviour of inverted pendulum structures during earthquakes. Bulletin of the Seismological Society of America 1963; 53: 404–417.